PHYSICAL REVIEW D **85,** 073001 (2012)

Zero temperature lattice Weinberg-Salam model for the values of the cutoff $\Lambda \sim 1$ TeV

M. A. Zubkov

ITEP, B. Cheremushkinskaya 25, Moscow, 117259, Russia

(Received 19 October 2011; published 2 April 2012)

The lattice Weinberg-Salam model at zero temperature is investigated numerically. We consider the model for the following values of the coupling constants: the Weinberg angle $\theta_W \sim 30°$, the fine structure constant $\alpha \sim (1/150)$, and the Higgs mass $M_H \sim 150$ GeV. We find that the fluctuational region begins at the values of the cutoff Λ above about 0.8 TeV. In this region the average distance between Nambu monopoles is close to their sizes. At $\Lambda > 1.1$ TeV the Nambu monopole currents percolate. Within the fluctuational region the considered definitions of the scalar field condensate give values that differ from the expected one $2M_z/g_z$. We consider the given results as an indication that the nonperturbative effects may be present in the Weinberg-Salam model at the large values of the cutoff. Our numerical results were obtained on the lattices of sizes up to $16^3 \times 32$.

DOI: 10.1103/PhysRevD.85.073001 PACS numbers: 12.15.−y, 11.15.Ha, 12.10.Dm

I. INTRODUCTION

Investigation of the phase transitions often requires the application of nonperturbative methods. In particular, the nonperturbative phenomena are important for the description of the finite temperature Electroweak phase transition [1–14]. At the same time, the phase diagram of the lattice Weinberg-Salam model at zero temperature also contains the phase transition [15–18]. The phase transition surface separates the Higgs phase from the symmetric phase. On both sides of the phase diagram it is necessary to find the way to approach continuum physics within the lattice model. It is expected that the continuum physics arises in some vicinity of this transition (on different sides of the transition different continuum models appear). Strictly speaking, this pattern is self-consistent only if the transition is of the second order. In this case close to the phase transition lattice spacing tends to zero and a kind of a continuum field theory appears. Indeed, zeroth order of the perturbation theory predicts the second order phase transition in the Weinberg-Salam model. However, already on the one-loop level the Coleman-Weinberg effective potential predicts the first order phase transition. This discrepancy points out to numerical lattice methods as to the judge. There may take place the 1st order phase transition or the 2nd order phase transition. Also another possibility appears: the transition may appear to be a crossover.

That is why we expect nonperturbative effects to appear in the lattice Weinberg-Salam model close to the transition between the two above mentioned phases. Or, in the other words, we expect nonperturbative effects to appear above some energy scale, because the increase of the energy scale corresponds to the decrease of the lattice spacing and, therefore, is achieved when the phase transition is approached. Based on trivial dimensional analysis we may expect that the mentioned scale can be compared to the electroweak scale ∼250 GeV. In fact, some indications were recently found that this scale might be around 1 TeV (see, for example, [19–25]). Namely, in the electroweak theory there exist objects that are not described by the first orders of the perturbation theory: Nambu monopoles and the Z-strings [26]. It has been found that there exists the vicinity of the phase transition [24], where the average distance between the Nambu monopoles is compared to their sizes. This region was called in [22] the fluctuational region (FR). Nambu monopoles may be considered as embryos of the unphysical phase within the physical one. Therefore, it is natural to suppose that within the FR both phases are mixed and neither the perturbation expansion around vacuum with zero scalar field nor the perturbation expansion around vacuum with nonzero scalar field cannot give the correct description of the situation. Besides, in [25] it was shown that there exist different ways to define scalar field condensate that give identical values out of the FR, and different values within the FR. On the boundary of the FR the lattice spacing a remains finite and practically does not depend on the lattice size (for the considered lattices). Actually, the value of the ultraviolet cutoff π/a on this boundary for the values of the Higgs boson mass 100 GeV, 150 GeV, 300 GeV is around 1 TeV. Thus the hypothesis suggested that above the energy scale 1 TeV in the Weinberg-Salam model nonperturbative effects may become important. It is worth mentioning that these effects, most likely, are related to the expansion in powers of λ while the first orders of the perturbation theory for the expansion in powers of α are expected to stay at work. In particular, no discrepancy was found between the renormalized fine structure constant and its one-loop estimate [25].

In this paper we extend the research of [25] to larger lattices (in [25] the lattices of sizes $8^3 \times 16$ were used; here we use lattices $16^3 \times 32$). In addition we investigate the properties of Nambu monopoles and Z-strings that were

*zubkov@itep.ru

out of the scope of the mentioned above papers. Namely, we consider their percolation properties that are related to their possible condensation. In the finite temperature theory it was found that the electroweak transition is accompanied with the condensation of the Nambu monopoles and the condensation of the Z-strings [27–29]. Here we find that in the zero-temperature model this occurs as well. The ''percolation transition'' in the Weinberg-Salam model at the values of couplings we consider is situated within the FR. And there exists the subregion of the FR, were both Z-strings and Nambu monopoles are condensed, while at least one of the considered definitions of the scalar field condensate still gives nonzero value.

This paper is organized as follows. In Sec. II we consider the definition of the lattice regularized Weinberg-Salam model and describe the details of the simulation. In Sec. III we discuss the phase diagram of the lattice model and the lines of constant physics. In Sec. IV we describe how lattice spacing was calculated in our study. In Sec. V we calculate the renormalized fine structure constant. In Sec. VI we investigate three different scalar field condensates. In Sec. VII we calculate Z-string and Nambu monopole percolation probabilities. In Sec. VIII we discuss the obtained numerical results. Throughout the paper the notations of differential forms on the lattice are used (for their definition see, for example, [30]).

II. THE LATTICE REGULARIZED WEINBERG-SALAM MODEL

We consider the Weinberg-Salam model without fermions. Its partition function has the form:

$$Z = \int DHD\Gamma \exp(-A(\Gamma, H)). \tag{1}$$

Here $A(\Gamma, H)$ is the action for the scalar doublet H and the gauge field $\Gamma = U \otimes e^{i\theta} \in SU(2) \otimes U(1)$:

$$\begin{aligned} A(\Gamma, H) = \beta \sum_{\text{plaquettes}} \left(\left(1 - \frac{1}{2}\,\mathrm{Tr} U_p\right) + \frac{1}{\mathrm{tg}^2\theta_W}(1 - \cos\theta_p) \right) \\ + \frac{\gamma}{2} \sum_{xy} |H_x - U_{xy} e^{i\theta_{xy}} H_y|^2 \\ + \sum_x (|H_x|^2(1 - 2\lambda - 4\gamma) + \lambda |H_x|^4). \end{aligned} \tag{2}$$

On the tree level we have:

$$\begin{aligned} v = \sqrt{2\frac{\gamma - \gamma_c}{\lambda}}, \qquad m_H = v\sqrt{\frac{8\lambda}{\gamma}}, \\ m_Z = v\sqrt{\frac{\gamma}{\beta \cos^2\theta_W}}, \qquad \gamma_c = \frac{1 - 2\lambda}{4}. \end{aligned} \tag{3}$$

Here we have introduced the vacuum expectation value v of $|H_x|$, the lattice Higgs boson mass $m_H = M_H a$, the lattice Z-boson mass $m_Z = M_Z a$, and the critical value γ_c.

After fixing unitary gauge

$$H = \begin{pmatrix} h \\ 0 \end{pmatrix}, \qquad h \in R, \tag{4}$$

where H is the scalar doublet, and the Z_2 gauge ambiguity remains $h_x \to (-1)^{n_x} h_x$, $Z \to [Z + \pi dn] \mathrm{mod} 2\pi$. Here the Z-boson field is defined as

$$Z = -\mathrm{Arg}[U_{11} e^{i\theta}]. \tag{5}$$

The tree-level approximation gives for the infrared effective constraint potential [25] after any Z_2 gauge is fixed:

$$V^{i-r}(\phi) = N_4 \lambda (\phi^2 - v^2)^2. \tag{6}$$

Here N_4 is the lattice volume.

In numerical simulations we use the Metropolis algorithm. The model is simulated in unitary gauge with the signs of h unfixed. After each 150 Metropolis sweeps the Z (or DZ) version of unitary gauge is fixed (for the definition of these gauges, see the next sections). As a starting point of our simulations on the lattice $16^3 \times 32$ we use configurations obtained on the lattice $8^3 \times 16$ during the preparation of [25]. Sixteen identical configurations are merged together forming the starting $16^3 \times 32$ configuration. Then, about 60 000 Metropolis sweeps are made before the measurement of observables begins (this required about 600 hours CPU time). During this preliminary run the 16 above mentioned parts of the lattice become decorrelated which signalizes that the thermalization is achieved.

III. PHASE DIAGRAM AND LINES OF CONSTANT PHYSICS

The lattice model defined by Eq. (2) has the four-dimensional $(\beta, \gamma, \lambda, \theta_W)$ phase diagram. On this phase diagram phase transition surface is three dimensional. The lines of constant physics on the tree level are the lines $[(\lambda/\gamma^2) = (1/8\beta)(M_H^2/M_W^2) = \text{const};\ \theta_W = \text{const}]$. We suppose that in the small vicinity of the transition the deviation of the lines of constant physics from the tree-level estimate may be significant. However, qualitatively their behavior is the same. Namely, the cutoff is increased along the line of constant physics when γ is decreased and the maximal value of the cutoff is achieved at the transition. Nambu monopole density in lattice units is also increased when the ultraviolet cutoff is increased.

In our lattice study we fix bare $\theta_W = \pi/6$, $\beta = 12$, $\lambda = 0.0025$. Therefore, strictly speaking we investigate the system along the line on the phase diagram that differs from the line of constant physics. This is illustrated by Fig. 1, where the projection of the phase diagram to the plane ($\beta = 12$, $\theta_W = \pi/6$) is drawn. This diagram is obtained, mainly, using the lattice $8^3 \times 16$. Some regions ($\lambda = 0.009$, required about 600 hours), however, were

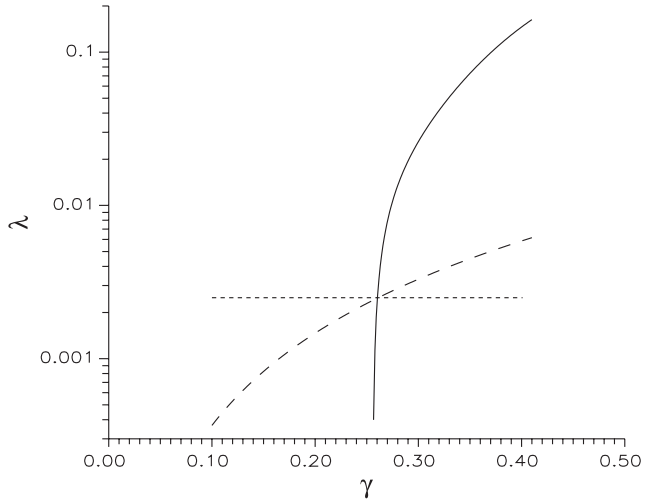

FIG. 1. The phase diagram of the model in the (γ, λ)-plane at $\beta = 12$. The dashed line is the tree-level estimate for the line of constant physics $((\lambda/\gamma^2) = (1/8\beta)(M_H^2/M_W^2) = \text{const})$ correspondent to bare $M_H^0 = 150$ GeV. The continuous line is the line of the phase transition between the physical Higgs phase and the unphysical symmetric phase (statistical errors for the values of γ at each λ on this line are about 0.005). The dotted line is the line $\lambda = 0.0025$. Along this line the physical quantities are calculated in the present research.

checked using larger lattices (see, for example, [19,20,22–24]). According to our data there is no dependence of the diagram on the lattice size. The physical Higgs phase is situated right to the solid transition line. The position of this line was determined using various methods [19,20,22–24]. However, the uncertainty is still present in the final determination of the phase transition points. This uncertainty on this figure is within the error bars of $\gamma = \gamma_c \pm 0.005$. The details of this uncertainty at $\lambda = 0.0025$ are discussed in the this paper (see below). The dashed line represents the tree-level estimate for the line of constant physics. The dotted line is the line $\lambda = 0.0025$. One can already see that on the tree level this straight line deviates from the line of constant physics. However, Fig. 1 demonstrates also that within the interval $\gamma \in [0.255, 0.27]$ (where the physical quantities are measured in the present research) the deviation of the tree-level estimate for the line of constant physics from the straight line $\lambda = 0.0025$ is not crucial. In fact, on the tree level along this straight line the fine structure constant does not vary. The renormalized fine structure constant is also almost not changed (see discussion below in Sec. V). As for the Higgs boson mass, its value on the tree level varies between 154 GeV at $\gamma = 0.255$ and 145 GeV at $\gamma = 0.27$. The variation of the renormalized Higgs mass along the line $\lambda = 0.0025$ is discussed in Sec. IV. Our data (with large statistical errors) also demonstrate that the Higgs mass does not deviate significantly from bare value $\sim$150 GeV at $\lambda = 0.0025$, $\gamma \in [0.2585, 0.27]$. It is worth mentioning that we did not investigate the renormalized W-boson mass in the present research. Therefore we do not represent here any data on the renormalized Weinberg angle. However, we also expect that it does not vary sufficiently at the considered values of γ.

In this paper we deal with the line $\lambda = 0.0025$, $\theta = \pi/6$, $\beta = 12$ for $\gamma \in [0.2585, 0.27]$ as with an approximation of the line of constant physics because along this line the main physical quantities (Higgs mass and fine structure constant) do not vary essentially. The lowest value $\gamma = 0.2585$ in the above mentioned interval is chosen because we expect that for the description of the model at $\gamma < 0.2585$ larger lattice sizes are necessary. This is related to the fact that at $\gamma < 0.2585$ the value of the cutoff is larger than 1.5 Tev and increases very fast [see discussion below in Sec. IV, Eq. (11)]. At the same time already for the values of the cutoff $\Lambda \sim 10$ TeV we need lattices of linear size $\gg 10$ (see discussion in Sec. VIII). We expect that the line of constant physics at $\Lambda \gg 1$ TeV deviates essentially from the straight line investigated in this paper. Not only may the Higgs mass deviate from its bare value but also the renormalized fine structure constant and, probably, the renormalized Weinberg angle may deviate from their bare values. However, for the investigation of such large values of Λ extremely large lattices are needed and such a research is out of the scope of this paper.

Below in this paper we deal with the investigation of the lattice model at fixed $\theta_W = \pi/6$, $\beta = 12$, $\lambda = 0.0025$. In Fig. 2 the data of the link part of the action $(1/4N_4)\sum_{xy} H_x^+ U_{xy} e^{i\theta_{xy}} H_y$ are represented. The dependence of the link part of the action on γ indicates that the phase transition (or a crossover) can be localized at $\gamma \sim \gamma_c' = 0.25775 \pm 0.00025$. (See also [25], where the same conclusion was made based on the data obtained on the lattice $8^3 \times 16$.) As in [25] we exclude the first order

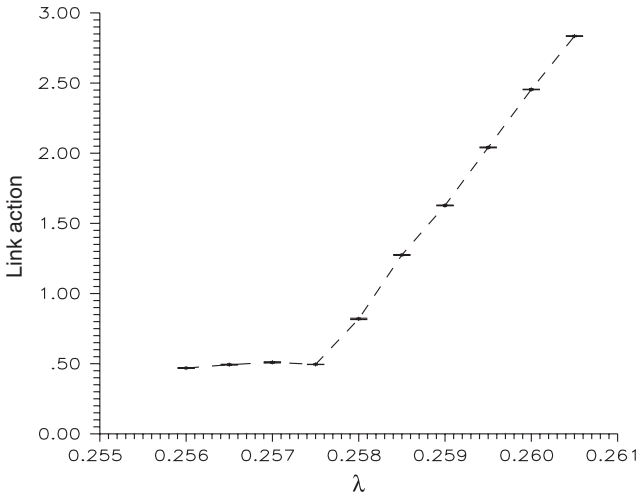

FIG. 2. The link part of the action as a function of γ at $\lambda = 0.0025$, $\beta = 12$ on the lattice $16^3 \times 32$.

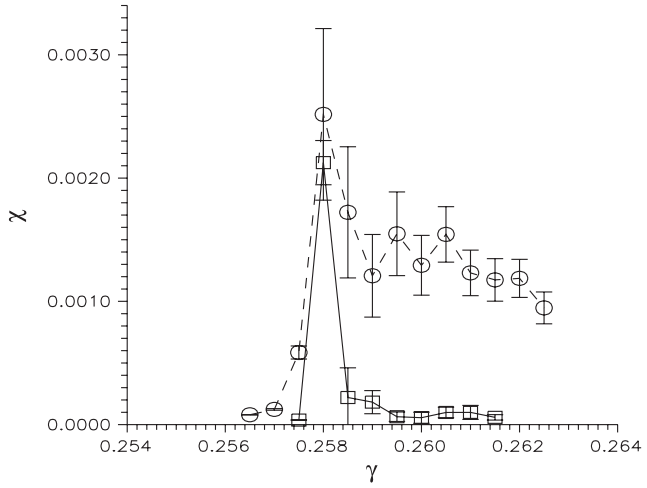

FIG. 3. Susceptibility χ (in lattice units) as a function of γ at $\beta = 12$, $\lambda = 0.0025$. Circles correspond to lattice $8^3 \times 16$ while squares correspond to lattice $16^3 \times 32$.

phase transition because we do not observe any sign of a two-state signal. In the next sections we shall demonstrate that the infrared UZ potential for the scalar field also points out to γ_c' as to the transition point.

In addition in Fig. 3 we represent the fluctuation of the zero momentum scalar field $\chi = [\delta H_{p=0}]^2 = \langle [H_{p=0}]^2 \rangle - \langle H_{p=0} >^2 \rangle$ in lattice units as a function of γ. Here $H_{p=0} = (1/N_4)\sum_x |H_x|$. From this plot we obtain the critical value $\gamma_c'' = 0.258 \pm 0.0005$. Moreover, the given plot indicates that we deal with the second order phase transition localized at γ_c''. Indeed, the values of the fluctuation $\delta H_{p=0}$ on the lattice $8^3 \times 16$ are about $\sqrt{2^4} = 4$ times larger than on the lattice $16^3 \times 32$ for $\gamma > \gamma_c''$. This means that for these values of γ the physical size of the lattice $8^3 \times 16$ is two times smaller than that of the lattice $16^3 \times 32$, as it should when the correlation length is smaller than the lattice size. However, at γ_c'' the fluctuations calculated using both lattices almost coincide with each other. This means that at $\gamma = \gamma_c''$ the physical sizes of both lattices are the same; that may happen only if the correlation length is much larger than the lattice size. It is worth mentioning that the difference between γ_c' and γ_c'' is 0.00025, which is within the statistical errors of both quantities.

It is worth mentioning that Fig. 3 allows us to estimate the fluctuation of the scalar field within the fluctuational region. On its boundary, at $\gamma = 0.2625$ (see below) we have $\chi \sim 0.001$ on the lattice $8^3 \times 16$. Also we know that at this value of γ the correlation length for the scalar field is about two lattice spacings. Therefore the given lattice contains $4^3 \times 8 = 512$ cubes of the linear size equal to the correlation length. This means that the fluctuation of the scalar field within such a cube is $\delta|H| \sim \sqrt{512 * \chi} \sim 0.7$ that is to be compared with the average value $\langle |H| \rangle \sim 2$. The formal requirement for the perturbation theory to be applied is $2 \sim \langle |H| \rangle \gg \delta|H| \sim 0.7$. It seems that this inequality is not satisfied. For $\gamma < 0.2625$ the situation is even worse. For example, at $\gamma = 0.26$ we have $\langle |H| \rangle \sim 2$ while $\delta|H| \sim 0.9$.

IV. Z-BOSON MASS, LATTICE SPACING, AND HIGGS BOSON MASS

For the calculation of the Z-boson mass we use the following definition of the Z-boson field:

$$Z_{xy} = Z_x^\mu = -[\mathrm{Arg}(\Phi_x^+ U_{xy} e^{i\theta_{xy}} \Phi_y)]. \quad (7)$$

Actually this definition of the Z-boson field coincides with the previous one (5) taken in the version of unitary gauge (4) with nonnegative h.

In order to evaluate the mass of the Z-boson we use the correlator:

$$\frac{1}{N^6} \sum_{\bar{x},\bar{y}} \left\langle \sum_\mu Z_x^\mu Z_y^\mu \right\rangle \sim e^{-m_Z |x_0 - y_0|} + e^{-m_Z (L - |x_0 - y_0|)}. \quad (8)$$

Here the summation $\sum_{\bar{x},\bar{y}}$ is over the three ''space'' components of the four vectors x and y while x_0, y_0 denote their ''time'' components. N is the lattice length in space direction. L is the lattice length in the time direction. The full lattice 4-volume is $N_4 = N^3 \times L$.

In order to evaluate the Higgs boson mass we use the correlator

$$\frac{1}{N^6} \sum_{\bar{x},\bar{y}} \{\langle |H_x||H_y| \rangle - \langle |H_x| \rangle^2\} \sim e^{-m_H |x_0 - y_0|} + e^{-m_H (L - |x_0 - y_0|)}. \quad (9)$$

We can roughly evaluate the dependence of the lattice Z-boson mass on the lattice size as follows. In finite temperature theory gauge boson thermal masses appear of the order of $m_g = M_g a \sim gTa \sim (g/N_T)$, where T is the temperature while N_T is the lattice size in imaginary time direction. Analogous to the finite temperature theory, this allows us to evaluate the finite volume contribution to the Z-boson mass as $\Delta m_Z \sim (g_Z/N)$, where N is the linear lattice size. For $\alpha \sim 1/150$, $N \sim 8$ we have $\Delta m_Z \sim 0.08$ while at $N \sim 16$ we expect $\Delta m_Z \sim 0.04$.

In Fig. 4 we represent our data on the Z-boson mass. Our numerical results confirm the results of [24]. Nonzero values of Z-boson mass are obtained at $\gamma \geq 0.2585$. At the same time for $\gamma \leq 0.258$ we observe large statistical errors for the ZZ correlator. Therefore, in this region of the phase diagram the Z-boson mass cannot be calculated and we suppose it vanishes somewhere between $\gamma = 0.25$ and $\gamma = \gamma_c'$.

Taking into account expression (3) for the Z-boson mass we use the following fit (γ_c is changed to $\tilde{\gamma}_c' = 0.2575$) to the data of Fig. 4:

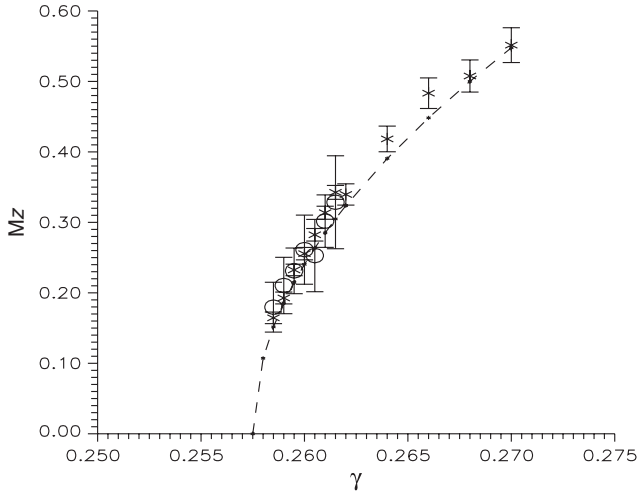

FIG. 4. Z-boson mass in lattice units as a function of γ at $\lambda = 0.0025$, $\beta = 12$. Crosses correspond to lattice $8^3 \times 16$. Circles correspond to lattice $16^3 \times 32$.

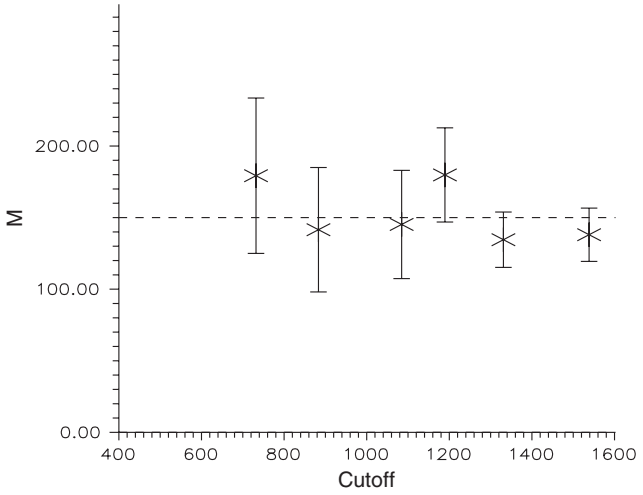

FIG. 5. Higgs boson mass in physical units as a function of the cutoff at $\lambda = 0.0025$, $\beta = 12$ on the lattice $8^3 \times 16$.

$$m_Z = \sqrt{\frac{2\gamma(\gamma - \tilde{\gamma}_c')}{\beta\lambda\cos^2\theta_W}}. \tag{10}$$

This fit is represented on the plot by the dashed line. It is worth mentioning that $\tilde{\gamma}_c'$ is within the error bars of γ_c'. We find that (10) with this value substituted instead of γ_c approximates the data better than with $\gamma_c' = 0.25775$ or $\gamma_c'' = 0.258$. This does not mean that Fig. 4 points out to $\tilde{\gamma}_c' = 0.2575$ as to the transition point instead of $\gamma_c' = 0.25775$. Instead, this means that there exist also other contributions to the dependence of the Z-boson mass on γ in addition to the tree-level estimate with the real critical value of γ substituted instead of its naive estimate.

Using the value of lattice Z-boson mass m_Z we can evaluate the ultraviolet cutoff $\Lambda = (\pi/a)$ as a function of γ via the relation $m_Z = a \times 91$ GeV. Further we shall use fit (10) in order to represent our results as a function of Λ. Namely, we use the following representation for Λ:

$$\Lambda = \pi\sqrt{\frac{\beta\lambda\cos^2\theta_W}{2\gamma(\gamma - 0.2575)}} * 91 \text{ GeV}. \tag{11}$$

In particular, in Fig. 5 we represent the Higgs boson mass calculated on the lattice $8^3 \times 16$ in physical units (in GeV) as a function of the cutoff. Unfortunately, we do not have enough statistics to calculate this mass on the larger lattices. We observe that the calculated values of the mass are close to the expected value $\sim$150 GeV. The deviation is within the statistical errors.

Our estimate for the ultraviolet cutoff at γ_c is $\sim$1 TeV. The value of Z-boson mass in lattice units at this point is about $\sim$0.2. The above mentioned estimate of the finite volume effect is $\sim$0.04. Therefore we expect that the values of the ultraviolet cutoff reported here cannot differ from that of obtained on an ideal infinite lattice by more than 20%. Thus we give here the following estimate for the cutoff Λ at $\gamma = \gamma_c$: $\Lambda_c = 1 \pm 0.02$ TeV.

V. RENORMALIZED FINE STRUCTURE CONSTANT

In order to calculate the renormalized fine structure constant $\alpha_{\mathrm{R}} = e^2/4\pi$ (where e is the electric charge) we use the correlator of Polyakov lines for the right-handed external leptons. These lines are placed along the selected direction (called below the imaginary time direction). The spacelike distance between the lines is denoted by R.

$$\mathcal{C}(|\bar{x} - \bar{y}|) = \langle \mathrm{Re}\Pi_t e^{2i\theta_{(\bar{x},t)(\bar{x},t+1)}} \Pi_t e^{-2i\theta_{(\bar{y},t)(\bar{y},t+1)}} \rangle \tag{12}$$

The potential is extracted from this correlator as follows:

$$\mathcal{V}(R) = -\tfrac{1}{L}\log\mathcal{C}(\mathrm{R}). \tag{13}$$

Here L is the size of the lattice in imaginary time direction.

Because of exchange by virtual photons and Z-bosons one would expect the appearance of the Coulomb and Yukawa interactions:

$$\mathcal{V}(r) = -\alpha_R\left[\mathcal{U}_0(r) + \frac{1}{3}\mathcal{U}_{m_Z}(r)\right] + \text{const},$$
$$\mathcal{U}_m(r) = -\frac{\pi}{N^3}\sum_{\bar{p}}\frac{e^{ip_3 r}}{\sin^2 p_1/2 + \sin^2 p_2/2 + \sin^2 p_3/2 + \mathrm{sh}^2 m/2}. \tag{14}$$

Here N is the lattice size, $p_i = \frac{2\pi}{L}k_i$, $k_i = 0, \ldots, L-1$.

We substitute to (14) the fit to the Z-boson mass represented in (10). The results are presented in Fig. 6 and are to be compared with the tree-level estimate for the fine structure constant $\alpha^{(0)} \sim (1/151)$ and the one-loop approximation (when we assume bare value of α to live at the scale $\sim$1 TeV while the renormalized value lives at the Electroweak scale M_Z): $\alpha^{(1)}(M_Z/1 \text{ TeV}) \sim \frac{1}{149.7}$.

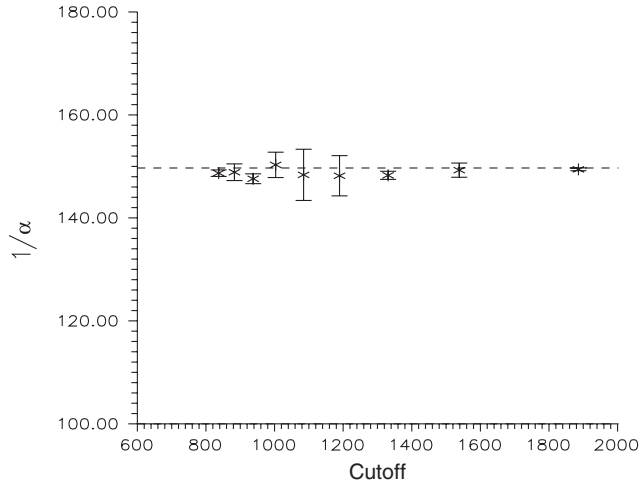

FIG. 6. The inverse renormalized fine structure constant $1/\alpha(M_Z/\Lambda)$ as a function of the cutoff Λ at $\lambda = 0.0025$, $\beta = 12$ on the lattice $16^3 \times 32$. The dashed line is the one-loop estimate for $\Lambda = 1$ TeV.

The values of the renormalized fine structure constant calculated on the lattice $16^3 \times 32$ are close to the values calculated on the lattice $8^3 \times 16$ represented in [25]. We observe that the renormalized fine structure constant calculated in the mentioned above way is rather close to the one-loop estimate (when the cutoff Λ in $\alpha^{(1)}(M_Z/\Lambda)$ is around 1 TeV. It is worth mentioning, that the present data on the renormalized fine structure constant (and the data of [25]) differ from that of reported in [24]. In [24] we used the potential extracted from the Wilson loops and approximated it by the simple $1/R$ fit. Moreover, in [24] the exchange by virtual Z-bosons was neglected. Therefore the values represented in [24] depend strongly on the lattice size and deviate essentially from the one-loop estimate near to the phase transition point.

VI. SCALAR FIELD CONDENSATE

In [25] three different effective constraint potentials were introduced. All them are defined in unitary gauge $H = \begin{pmatrix} h \\ 0 \end{pmatrix}$ with real h. The first one is the ultraviolet potential

$$\exp(-V^{u-v}(\phi)) = \langle \delta(\phi - h_x) \rangle. \tag{15}$$

Here real scalar field h_x is defined on the lattice points x.

In order to define the infrared potential

$$\exp(-V^{i-r}(\phi)) = \left\langle \delta\left(\phi - \frac{1}{N_4}\sum_x h_x\right)\right\rangle, \tag{16}$$

(where N_4 is the number of lattice points) it is necessary to fix the ambiguity

$$h_x \to (-1)^{n_x} h_x, \qquad Z \to [Z + \pi d n] \mathrm{mod} 2\pi, \tag{17}$$

where the Z-boson field is defined in (5).

The first way is minimization of

$$\sum_{\text{links}} (1 - \cos Z) \to \min \tag{18}$$

with respect to the mentioned Z_2 transformations. In [25] this gauge was called the Z version of the unitary gauge and the corresponding effective potential (16) is called the UZ potential.

The second way to define the unitary gauge with $h_x \in R$ is to minimize the divergence of Z with respect to the remaining Z_2 transformations:

$$\sum_x [\delta Z]^2 \to \min. \tag{19}$$

This gauge is called the DZ version of the unitary gauge and the corresponding effective potential (16) is called UDZ potential.

The three above mentioned effective potentials give three different definitions of the scalar filed condensate. (The condensate v is defined as the value of ϕ, at which the potential $V(\phi)$ has its minimum).

In Fig. 7 we represent these three condensates as functions of the cutoff $\Lambda = \frac{\pi}{a}$. We consider the condensates in physical units, i.e. we multiply the values expressed in lattice units by $\sqrt{\gamma}/a$. So, we define $v^{\text{phys}} = (\sqrt{\gamma}/a)v$.

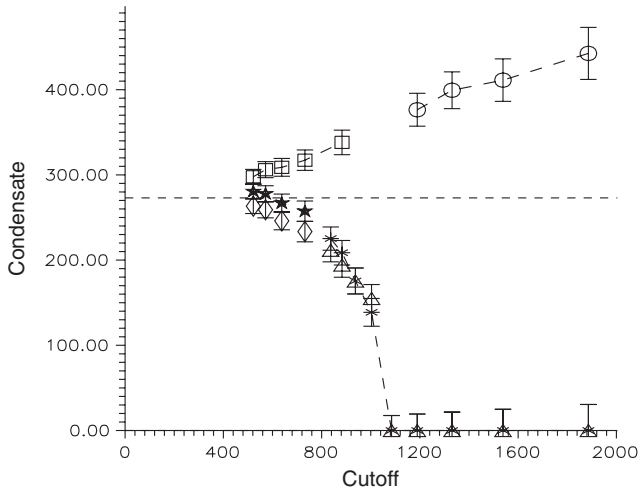

FIG. 7. The scalar field condensate (in GeV) as a function of the cutoff for $\lambda = 0.0025$, $\beta = 12$. Circles correspond to the UZ potential, lattice $16^3 \times 32$. Empty squares correspond to the UZ potential, lattice $8^3 \times 16$. Crosses correspond to the UDZ potential, lattice $16^3 \times 32$. Stars correspond to the UDZ potential, lattice $8^3 \times 16$. Triangles correspond to the ultraviolet potential, lattice $16^3 \times 32$. Diamonds correspond to the ultraviolet potential, lattice $8^3 \times 16$.

The scalar field condensate (in physical units) has to be renormalized. The renormalized condensate is usually defined as $v_R^{\rm phys} = (1/Z_H^{[1/2]})v^{\rm phys}$, where the wave function renormalization constant enters the following approximation for the scalar field propagator:

$$\langle [H_p]^+ H_q\rangle - |\langle H\rangle|^2 = Z_H \frac{\delta_{pq}}{N_4(4\sum_i \sin^2 p/2 + 4{\rm sh}^2\frac{m_H}{2})}. \quad (20)$$

Here $H_p = (1/N_4)\sum_x e^{ipx}H_x$, and $N_4 = N^3L$.

Because of the renormalizability the Z-boson mass is related to the scalar field condensate as follows: $M_Z = g_Z v_R^{\rm phys}/2 = (1/Z_H^{[1/2]})g_Z v^{\rm phys}/2$, where $g_Z = (4\sqrt{\pi\alpha})/(\sin 2\theta_W)$ is the renormalized coupling constant. In the perturbation theory the deviation of Z_H from unity is proportional to the factor $\sim\alpha\log(\Lambda/M_Z) \sim 0.02$ (for $\Lambda \sim 1$ TeV). Therefore, for $\Lambda \sim 1$ TeV we expect $Z_H \sim 1$.

That is why the perturbation theory prompts that both the (nonrenormalized) scalar field condensate (represented in Fig. 7) and the renormalized one must be close to the value $v_0^{\rm phys} = 2M_Z/g_Z = \sin 2\theta_W M_Z/\sqrt{4\pi\alpha} \sim 273$ GeV (this value differs from the conventional value 246 GeV due to the difference in α). We observe that all considered condensates approach this value when the cutoff is decreased. However, an essential deviation from this value appears at the values of the cutoff $\sim$1 TeV. Looking at this plot we also conclude that the condensates extracted from the UDZ potential and from the ultraviolet potential represent close quantities.[1] At the same time the UZ potential gives different value of the scalar field condensate. At the present moment we do not understand what is the reason for such a behavior. It is worth mentioning that the condensate extracted from the UZ potential vanishes at γ_c' (see Fig. 8). We must remember, that the cutoff was not calculated at this point but Fig. 3 indicates that at this point we may have $\Lambda_c' \sim \infty$. (Let us remind also that Fig. 2 points out to γ_c' as to the phase transition point.) The other two condensates vanish at $\Lambda_c \sim 1$ TeV, i.e. at $\gamma_c = 0.26075 \pm 0.00005$, where the value of the cutoff has been calculated explicitly. We shall see in the next section that close to this point of the phase diagram both the Z-string and the Nambu monopoles begin to percolate.

The observed behavior of the scalar field condensates calculated in UZ and UDZ versions of unitary gauge means that the wave function renormalization constant for the scalar field (defined in these gauges) differs from the perturbation theory prediction at $\Lambda > 800$ GeV. (We may calculate this constant as $Z_H = (273\,{\rm GeV}/{\rm v}^{\rm phys})^2$, where $v^{\rm phys}$ is drawn in Fig. 7.)

[1]For $\Lambda < 0.8$ TeV we do not have data from the lattice $16^3 \times 32$. Therefore for these values of the cutoff we represent on the plot the data obtained on the lattice $8^3 \times 16$.

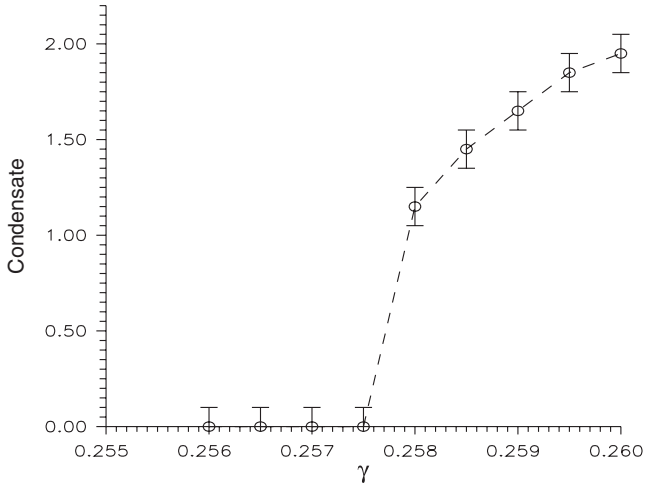

FIG. 8. The scalar field condensate extracted from the UZ potential in lattice units as a function of γ for $\lambda = 0.0025$, $\beta = 12$ on the lattice $16^3 \times 32$.

VII. Z-STRINGS AND NAMBU MONOPOLES

In this section we use definition (7) of the Z-boson field. The classical solution corresponding to a Z-string should be formed around the two-dimensional topological defect which is represented by the integer-valued field defined on the dual lattice $\Sigma = (1/2\pi)^*([dZ_{{\rm mod}2\pi} - dZ)$. Therefore, Σ can be treated as the worldsheet of a *quantum* Z-string [27]. Then, the worldlines of quantum Nambu monopoles appear as the boundary of the Z-string worldsheet $j_Z = \delta\Sigma$.

The percolation probability of Nambu monopoles is defined as follows. First let us denote the probability that two points x, y are connected by the monopole cluster by $\rho(x, y)$. We may identify it with the following quantity

$$\langle \Psi_x^+ \Psi_y\rangle = \rho(x, y), \quad (21)$$

where operator Ψ_x^+ creates the monopole-antimonopole pair at the point x. This identification allows us to calculate the lightest monopolium mass m_M, i.e. the mass of the quantum state consisted of the monopole-antimonopole pair connected by the Z-string

$$\Pi_1(|x_0 - y_0|) = \frac{1}{N^6}\sum_{x_1,x_2,x_3,y_1,y_2,y_3}\langle \Psi_x^+\Psi_y\rangle \sim A(e^{-m_M|x_0-y_0|} + e^{-m_M(L-|x_0-y_0|)}). \quad (22)$$

Here the lattice size is $N^3 \times L$, and it is implied that the mass is calculated in the region of the phase diagram, where the condensate of Ψ vanishes. In order to calculate this condensate we consider the following quantity:

$$\Pi_3(|\bar{x} - \bar{y}|) = \frac{1}{N^2}\sum_{x_3,y_3}\langle \Psi^+_{(\bar{x},x_3)}\Psi_{(\bar{y},y_3)}\rangle \sim |\langle\Psi\rangle|^2 + \tilde{\Pi}_3(|\bar{x} - \bar{y}|), \quad (23)$$

where $\bar{x} = (x_0, x_1, x_2)$, and $\tilde{\Pi}_3(r) \to 0 (r \to \infty)$. Thus the condensate is defined through the percolation probability $C_{\text{mon}} = |\langle\Psi\rangle|^2 = \lim_{r\to\infty}\Pi_3(r)$. It is worth mentioning that the two quantities $\Pi_1(r)$ and $\Pi_3(r)$ give different values at $r \to \infty$ if there is the massless scalar excitation in the spectrum, otherwise $\Pi_1(r) - \Pi_3(r) \to 0 (r \to \infty)$.

In a similar way we are also able to calculate the mass of the lightest excitation of the Z-string. First, the probability of the two points to be connected by the Z-string cluster is defined. Next, this probability is related to the two-point correlator of the operators that create the Z-string excitations. After that the mass of the lightest excitation is extracted and the percolation probability for the Z-strings is defined. The percolation probabilities for the Nambu monopoles and the Z-strings are represented in Fig. 9. We observe that both monopole currents and Z-string worldsheets percolate at $\Lambda > 1.1$ TeV.

The monopolium mass and the lightest Z-string excitation mass calculated are represented in Fig. 10 as functions of the cutoff. One can see, that both these masses decrease when the cutoff is increased. At $\Lambda > 1.1$ TeV we do not calculate the mentioned masses because the condensates of the monopolium and of the Z-string excitations appear.

The code for the calculation of the percolation probability was written especially for the investigation reported in this paper. It has been tested in several ways. In particular, results of [28,29] were reproduced.

According to the classical picture the Nambu monopole size is of the order of M_H^{-1}. Therefore, for example, for $a^{-1} \sim 250$ GeV and $M_H \sim 150$ GeV the expected size of the monopole is about two lattice spacings. The monopole density around 0.015 means that among about 16 sites there exists 1 site that is occupied by the monopole.

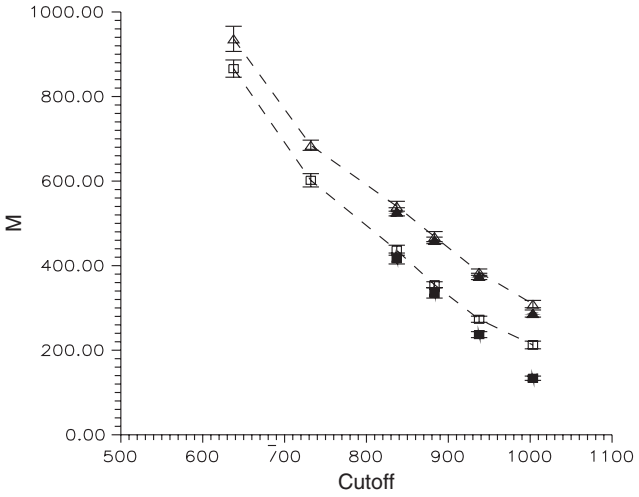

FIG. 10. The monopolium mass (triangles) and the lightest string excitation mass (squares) as a function of the cutoff calculated at $\lambda = 0.0025$, $\beta = 12$ on the lattice $8^3 \times 16$ (empty symbols) and $16^3 \times 32$ (dark symbols).

Average distance between the two monopoles is, therefore, about 2 lattice spacings that is the monopole size. In Fig. 11 (where the Nambu monopole density is represented as a function of the cutoff) we observe, that at $\Lambda > \Lambda_{c2} \sim 0.8$ TeV the Nambu monopole density is larger than 0.015, i.e. the average distance between monopoles is less then the classical monopole size. According to [24] this means that at Λ_{c2} we enter the fluctuational region. It is worth mentioning that within this region the notion of quantum Nambu monopole differs from the notion of the classical Nambu monopole considered in [26]. In particular, the size of the quantum object may be sufficiently less than that of the classical Nambu monopole.

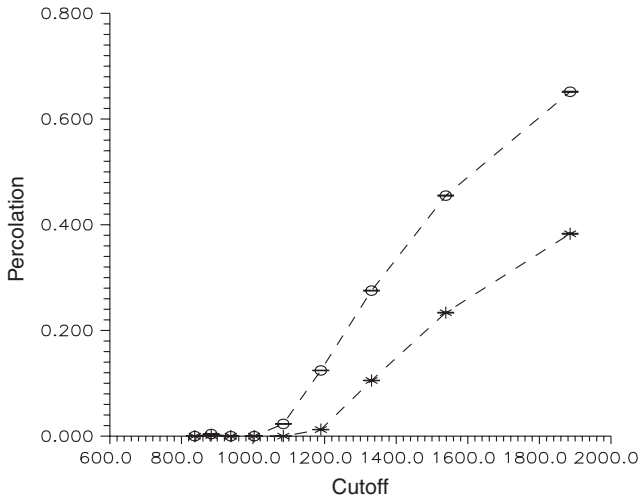

FIG. 9. The percolation probability for the Z-string (circles) and for the Nambu monopoles (crosses) as a function of the cutoff $\Lambda = \frac{\pi}{a}$ (in GeV) at $\lambda = 0.0025$, $\beta = 12$ on the lattice $16^3 \times 32$.

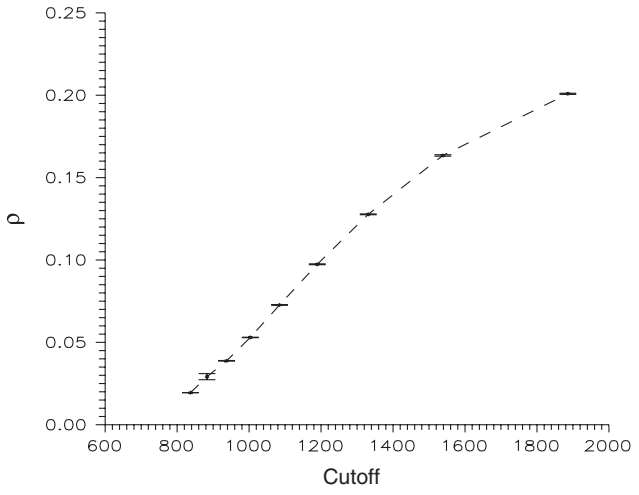

FIG. 11. The Nambu monopole density (in lattice units) as a function of the cutoff at $\lambda = 0.0025$, $\beta = 12$ on the lattice $16^3 \times 32$.

The original estimate of the Nambu monopole mass was given by Nambu [26]:

$$M_N \sim \frac{4\pi}{3e}\sin^{(5/2)}\theta_W\sqrt{\frac{M_H}{M_W}}246\ \text{GeV} \sim 900\ \text{GeV}. \quad (24)$$

Then, according to [26] the classical energy of monopole-antimonopole pair is

$$E = 2M_M - \frac{Q^2}{4\pi l}, \quad (25)$$

where $Q = (4\pi)/(e\sin^2\theta_W)$ is the monopole charge while l is the average distance between the monopoles in the monopolium. We can use this formula to estimate roughly the dependence of the monopolium mass on the cutoff. At small values of Λ the contribution of the $1/l$ term can be neglected (as the monopole density is negligible) and the lightest monopolium mass is expected to be close to the value $\sim$1.8 TeV. However, when the cutoff is increased, the average distance between Nambu monopoles is decreased. Therefore, l in (25) is decreased as well. As a result the monopolium mass is decreased. Indeed, we observe this kind of behavior in Fig. 10.

It is worth mentioning that the monopolium and the Nambu monopole itself are unstable as classical objects [26]. However, when the cutoff is increased, the whole picture of Nambu monopoles and monopolium is changed. The operator [defined in (21)] that creates the monopole-antimonopole pair actually creates the quasiparticle, the properties of which may differ essentially from the properties of the classical monopolium. In particular, these quasiparticles are condensed at $\Lambda > 1.1$ TeV.

VIII. DISCUSSION

Let us try to estimate the conditions under which the perturbation theory can be applied to this model. We make this estimate in the spirit of Vol. 5, paragraph 146 of [31] (where the similar considerations were used in order to estimate the width of the fluctuational region in the finite temperature Ginzburg-Landau model). We are going to compare the vacuum average of H with the fluctuations of H within the 4-volume N_4, the linear size of which is equal to the correlation length of H. This correlation length in lattice units is equal to $1/m_H$. The fluctuations are obtained from (6) and are of the order of $\delta H \sim (1/v\sqrt{8N_4\lambda}) \sim (m_H^2/v\sqrt{8\lambda})$. Therefore, at $v \gg (m_H^2/v\sqrt{8\lambda})$ the perturbation theory can be applied while otherwise it might not be applied. Finally, we obtain $\lambda \ll \gamma^2/8$ or $\frac{m_H}{m_W}\sqrt{4\pi\alpha} \ll 1$. For $m_H \sim 150$ GeV and $\alpha \sim 1/150$ this expression reads $0.54 \ll 1$. This estimate is indeed confirmed by numerical results (see the end of Sec. II). Thus already on this level there may appear some doubts about the validity of the perturbation expansion within the given model.

Above we have reported the results of our numerical investigation of lattice Weinberg-Salam model at $\beta = 12$, $\lambda = 0.0025$, $\theta_W = 30°$. For these values of couplings the bare Higgs boson mass is close to 150 GeV near to the transition between the Higgs phase and the symmetric phase. Numerical simulations were performed on the lattices of sizes up to $16^3 \times 32$.

Our data draw the following pattern of the phase transition:

(1) When the cutoff is increased (γ is decreased) Z vortices become more and more dense. Somewhere around $\Lambda \sim 0.8$ TeV ($\gamma_{c2} \sim 0.2625$) the transition to the fluctuational region occurs [24]. In this region Z-vortices and the Nambu monopoles dominate. The average distance between Nambu monopoles becomes compared to their sizes.

(2) At the value of Λ around $\Lambda_c \sim 1$ TeV (γ around $\gamma_c \sim 0.26075$) the scalar field condensates calculated using the UDZ effective potential and the ultraviolet effective potential vanish. At $\Lambda >$ 1.1 Tev the Nambu monopoles and the Z-strings begin to percolate. This means, in particular, that the operator that (naively) creates the so-called monopolium state actually creates the quasiparticles that are condensed.

(3) At the value of γ around $\gamma_c' \sim 0.25775$ the scalar field condensate calculated using the UZ effective potential vanishes. Also somewhere close to γ_c' the derivative of the link part of the action has the steplike discontinuity. We cannot calculate the ultraviolet cutoff at γ_c' due to large statistical errors. At the present moment we do not exclude that it tends to infinity at this point on the ideal infinite lattice.

The technical question about the order of the phase transition remains. There still exist two possibilities: either we deal with the second order phase transition (localized at γ_c') or with the crossover. The first possibility is realized if at γ_c' all lattice masses vanish or the correlation lengths are infinite at this point. The behavior of the scalar field fluctuation indicates that this may indeed be true. However, accurate investigation of the lattice masses is still to be performed in the vicinity of γ_c'. Let us now estimate the lattice size needed for such an investigation. Suppose, we need to investigate the region of the phase diagram with $\Lambda = (\pi/a) \sim 1$ TeV. Then, the lattice size has to be much larger than the correlation length: $L \gg (1/m_H) = (1/150\ \text{GeV}a) \sim 2$. Therefore, the lattices of sizes $16^3 \times 32$ seem to us large enough to investigate the model at $\gamma \geq 0.2585$. If, however, we are going to investigate the region of the phase diagram with $\Lambda \sim 10$ TeV, we need to have lattices of sizes $L \gg 10$. For this purpose lattices used in the present research are not large enough. That's why if the second order phase transition is indeed present at γ_c', in a small vicinity of this point, where

$\Lambda \gg 1$ TeV (most likely, this vicinity is situated within the interval [0.2575, 0.2585], the numerical lattice methods that use lattices of sizes up to $16^3 \times 32$ cannot be applied for the calculation of lattice masses.

The scalar field condensates calculated in three different ways in our study differ from each other and from the expected value $\sim$273 GeV for the values of $\Lambda > 800$ GeV. However, all them have tendencies to approach this value when Λ is decreased. This means that the wave function renormalization constant for the scalar field differs from its perturbative estimate at $\Lambda > 800$ GeV. The percolation probability for the Nambu monopoles and for the Z-strings differ from zero at $\Lambda > 1$ TeV. We consider this behavior as a manifestation of the nonperturbative effects present in the given model at large enough energy scales. It is worth mentioning that the point of view that the nonperturbative effects may become important in the Higgs sector of the standard model is not new. In particular, in [32] it was argued that the wave function renormalization constant for the scalar field contains large nonperturbative contribution (at zero temperature). This conclusion of [32] is in accordance with our results represented here.

The situation seems to us similar to the phase transition in the second order superconductors at finite temperature. Namely, there exists the fluctuational region around the critical temperature $(T_c - \Delta T; T_c + \Delta T)$, where the perturbation theory cannot be applied and the nonperturbative effects are present [31]. In the lattice Weinberg-Salam model (at zero temperature) there also exists such a region around the phase transition at γ'_c. This region is localized within the interval $[\gamma'_c; \gamma_{c2}]$ that corresponds to values of the cutoff $\Lambda > 0.8$ TeV. As it was explained above we observe indications that within this region nonperturbative effects become important.

ACKNOWLEDGMENTS

The author kindly acknowledges discussions with M. I. Polikarpov, P. Buividovich, and E. Luschevskaya. This work was partly supported by RFBR Grants No. 09-02-00338 and No. 11-02-01227, and by the Grant for Leading Scientific Schools No. 679.2008.2. This work was also supported by the Federal Special-Purpose Programme ''Cadres'' of the Russian Ministry of Science and Education. The numerical simulations have been performed using the facilities of Moscow Joint Supercomputer Center, the supercomputer center of Moscow University, and the supercomputer center of Kurchatov Institute.

[1] F. Csikor, Z. Fodor, and J. Heitger, Phys. Rev. Lett. **82**, 21 (1999); Phys. Rev. D **58**, 094504 (1998); Nucl. Phys. B, Proc. Suppl. **63**, 569 (1998).
[2] F. Csikor, Z. Fodor, and J. Heitger, Phys. Lett. B **441**, 354 (1998).
[3] F. Csikor, Z. Fodor, J. Hein, A. Jaster, and I. Montvay, Nucl. Phys. **B474**, 421 (1996).
[4] Joachim Hein and Jochen Heitger (DESY Collaboration) Phys. Lett. B **385**, 242 (1996).
[5] F. Csikor, Z. Fodor, J. Hein, J. Heitger, A. Jaster, and I. Montvay, Nucl. Phys. B, Proc. Suppl. **53**, 612 (1997).
[6] Z. Fodor, J. Hein, K. Jansen, A. Jaster, and I. Montvay, Nucl. Phys. **B439**, 147 (1995).
[7] F. Csikor, Z. Fodor, J. Hein, and J. Heitger, Phys. Lett. B **357**, 156 (1995).
[8] F. Csikor, Z. Fodor, J. Hein, K. Jansen, A. Jaster, and I. Montvay, Nucl. Phys. B, Proc. Suppl. **42**, 569 (1995).
[9] F. Csikor, Z. Fodor, J. Hein, K. Jansen, A. Jaster, and I. Montvay, Phys. Lett. B **334**, 405 (1994).
[10] Y. Aoki, F. Csikor, Z. Fodor, and A. Ukawa, Phys. Rev. D **60**, 013001 (1999); Nucl. Phys. B, Proc. Suppl. **73**, 656 (1999).
[11] Y. Aoki, Phys. Rev. D **56**, 3860 (1997).
[12] Karl Jansen, Nucl. Phys. B, Proc. Suppl. **47**, 196 (1996).
[13] Zoltan Fodor and Karl Jansen, Phys. Lett. B **331**, 119 (1994).
[14] M. Gurtler, E.-M. Ilgenfritz, and A. Schiller, Phys. Rev. D **56**, 3888 (1997); K. Rummukainen, M. Tsypin, K. Kajantie, M. Laine, and M. Shaposhnikov, Nucl. Phys. **B532**, 283 (1998); Yasumichi Aoki, Phys. Rev. D **56**, 3860 (1997); N. Tetradis, Nucl. Phys. **B488**, 92 (1997); B. Bunk, E.-M. Ilgenfritz, J. Kripfganz, and A. Schiller, Nucl. Phys. **B403**, 453 (1993); Phys. Lett. B **284**, 371 (1992).
[15] I. Montvay, Nucl. Phys. **B269**, 170 (1986).
[16] W. Langguth and I. Montvay, Z. Phys. C **36**, 725 (1987).
[17] Anna Hasenfratz and Thomas Neuhaus, Nucl. Phys. **B297**, 205 (1988).
[18] W. Langguth, I. Montvay, and P. Weisz, Nucl. Phys. **B277**, 11 (1986).
[19] M. A. Zubkov and A. I. Veselov, J. High Energy Phys. 12 (2008) 109.
[20] A. I. Veselov and M. A. Zubkov, Proc. Sci., LAT2009 (2009) 214.
[21] B. L. G. Bakker, A. I. Veselov, and M. A. Zubkov, in *13th International Conference on Selected Problems of Modern Theoretical Physics (SPMTP08)*, (Joint Institute for Nuclear Research, Dubna, 2008).
[22] M. A. Zubkov, Phys. Lett. B **684**, 141 (2010).
[23] M. A. Zubkov, arXiv:1007.4885.
[24] M. A. Zubkov, Phys. Rev. D **82**, 093010 2010.
[25] M. I. Polikarpov and M. A. Zubkov, Phys. Lett. B **700**, 336 (2011).
[26] Y. Nambu, Nucl. Phys. **B130**, 505 (1977); A. Achucarro and T. Vachaspati, Phys. Rep. **327**, 347 (2000); Phys. Rep. **327**, 347 (2000).
[27] M. N. Chernodub, JETP Lett. **66**, 605 (1997).

[28] M. N. Chernodub, F. V. Gubarev, E. M. Ilgenfritz, and A. Schiller, Phys. Lett. B **434**, 83 (1998); Phys. Lett. B **443**, 244 (1998).

[29] B. L. G. Bakker, A. I. Veselov, and M. A. Zubkov, Phys. Lett. B **642**:147(2006).

[30] M. I. Polikarpov, U. J. Wiese, and M. A. Zubkov, Phys. Lett. B **309**, 133 (1993).

[31] L. D. Landau and E. M. Lifshitz, *Course of Theoretical Physics* (Pergamon, New York, 1980).

[32] P. Cea, M. Consoli, and L. Cosmai, arXiv:hep-lat/0407024; M. Consoli and P. M. Stevenson, Z. Phys. C **63**, 427 (1994); Phys. Lett. B **391**, 144 (1997); Int. J. Mod. Phys. A **15**, 133 (2000); P. Cea, M. Consoli, and L. Cosmai, Mod. Phys. Lett. A **13**, 2368 (1998); P. Cea, M. Consoli, L. Cosmai, and P. M. Stevenson, Mod. Phys. Lett. A **14**, 1673 (1999); Nucl. Phys. B, Proc. Suppl. **83**, 660 (2000).